Trajectory-Based Representation of Human Actions

Antonios Oikonomopoulos[1], Ioannis Patras[2], Maja Pantic[1],
and Nikos Paragios[3]

[1]Imperial College London, 180 Queensgate, SW7 2AZ London, UK
{aoikonom,m.pantic}@imperial.ac.uk
[2]Department of Electronic Engineering, Queen Mary University, London, UK
I.Patras@elec.qmul.ac.uk
[3]Ecole Centrale de Paris, Grande Voie des Vignes, 92 295 Chatenay-Malabry, France
nikos.paragios@ecp.fr

Abstract. This work addresses the problem of human action recognition by introducing a representation of a human action as a collection of short trajectories that are extracted in areas of the scene with significant amount of visual activity. The trajectories are extracted by an auxiliary particle filtering tracking scheme that is initialized at points that are considered salient both in space and time. The spatiotemporal salient points are detected by measuring the variations in the information content of pixel neighborhoods in space and time. We implement an online background estimation algorithm in order to deal with inadequate localization of the salient points on the moving parts in the scene, and to improve the overall performance of the particle filter tracking scheme. We use a variant of the Longest Common Subsequence algorithm (LCSS) in order to compare different sets of trajectories corresponding to different actions. We use Relevance Vector Machines (RVM) in order to address the classification problem. We propose new kernels for use by the RVM, which are specifically tailored to the proposed representation of short trajectories. The basis of these kernels is the modified LCSS distance of the previous step. We present results on real image sequences from a small database depicting people performing 12 aerobic exercises.

1 Introduction

With an ever-increasing role of computers and other digital devices in our society, one of the main foci of the research in Artificial Intelligence should be on Emerging Human-Machine Systems. A related, crucial issue is that of Human-Machine Interaction (HMI). A long-term goal in HMI research is to approach the naturalness of human-human interaction. This means integrating 'natural' means that humans employ to interact with each other into the HMI designs. With this motivation, automatic speech recognition and synthesis have been the topics of research for decades. Recently, other human interactive modalities such as facial and body gestures have also gained interest as potential modes of HMI. The analysis of what is present in a scene is an essential issue in the

T.S. Huang et al. (Eds.): Human Computing, LNAI 4451, pp. 133–154, 2007.

development of natural Human-Machine interfaces. Who is in the scene, what is (s)he doing, and how is (s)he doing it, are essential questions that should be answered if natural interfaces that are non-obtrusive and informative for the user are to be realized. Vision offers the means to achieve this. It also represents an essential link to the creation of systems which are able to adapt to the affective state of their user, leading in this way to an affect-sensitive interaction between the user and the machine. Particularly for ambient intelligence, anticipatory interfaces, and human computing, the key is the ease of use - the ability to unobtrusively sense certain behavioral cues of the users and to adapt automatically to their typical behavioral patterns and the context in which they act [1]. Sensing and interpretation of human behavioral cues play an important role and are extremely relevant for the development of applications in the fields of security (video surveillance and monitoring), natural multimodal interfaces, augmented reality, smart rooms, object-based video compression and driver assistance. Tremendous amount of work has been done in the field in recent years [2],[3].

In this work we present an unsupervised method for the representation of the activity taking place in a scene. This method is based on the detection of salient points in space and time, that correspond to regions with a significant amount of activity. Subsequently, we track these points in time using a state-estimation approach in order to reach a representation based on short trajectories. We test the proposed method using real image sequences of subjects performing several aerobic exercises. It can be used, however, to represent any type of activity, including hand gestures, gait, extraction of motion patterns etc. Possible applications lie in the area of e-health, where the development of non-stationary, non-intrusive, non-invasive monitoring inside and outside the clinical environment is essential, due to demanding patients, aging population and rising costs. The method can be realized as an adaptive system that will be able to monitor and assess the correctness of the performed exercise, and will provide an appropriate alternative (senior) fitness plan, assisting in this way nurses,physical therapists and family members. The system can also be configured for use at home, to accommodate elderly but otherwise healthy patients or patients suffering from conditions like rheumatism and chronic pain.

2 Related Work

2.1 Tracking

The main objective of tracking is to estimate the state x_k (e.g. position, pose) given all the measurements $z_{1:k}$ up to the current time instant k. In a probabilistic framework, this translates in the construction of the a posteriori probability $p(x_k|z_{1:k})$. Theoretically, the optimal solution in case of Gaussian noise in the measurements is given by the Kalman filter [4], which yields the posterior being also Gaussian. Kalman filters and their variants, like the Extended (EKF) and the Unscented Kalman Filters (UKF) [5], [6], [7] have been extensively used for a variety of tracking applications [8], [9]. However, in nonlinear and non-Gaussian state estimation problems Kalman filters can be significantly off.

To overcome the limitations of Kalman filtering, the classical particle filtering algorithm, or so-called Condensation algorithm was proposed [10], [11]. The main idea behind particle filtering is to maintain a set of possible solutions called particles. Each particle is associated with a weight, the latter expressing the likelihood of the particle being the actual solution. By maintaining a set of solutions instead of a single estimate as is done by Kalman filtering, particle filters are more robust to missing and inaccurate data. The major drawback of the classic Condensation algorithm, however, is that a large amount of particles might be wasted because they are propagated into areas with small likelihood. In order to overcome this problem, a number of variants to the original algorithm have been proposed, having as a common characteristic the goal of achieving a more optimal allocation of new particles. Since particle weights determine how the particles are being resampled, the likelihood function has an essential influence on the tracking performance [12]. Several attempts have been made in order to adjust the way new particles are assigned, through the use of kernels [13], [14], [15], orientation histograms [16] or special transformations like Mean Shift [17].

Despite the improvement in the tracking performance of the previous methods, the inherent problem of the classic condensation algorithm, that is, the propagation of particles in areas of small likelihood is not sufficiently addressed. In order to effectively deal with this issue, the Auxiliary Particle Filtering (APF) algorithm was proposed by Pitt and Shephard [18]. The APF algorithm operates in two steps. At first, particles are propagated and their likelihood is evaluated. Subsequently, the algorithm chooses again and propagates the particles according to the likelihood of the previous step. Since the introduction of the APF algorithm, a number of variants have been proposed in order to address different issues. In [19] a modified APF tracking scheme is proposed for the tracking of deformable facial features, like mouth and eye corners. The method uses an invariant color distance that incorporates a shape deformation term as an observation model to deal with the deformations of the face. In order to take into account spatial constraints between tracked points, the particle filter with factorized likelihoods is proposed in [20], where the spatial constraints between different facial features are pre-learned and the proposed scheme tracks constellations of points instead of a single point, by taking into account these constraints.

Particle filters are often used within a template tracking framework. The object's appearance is captured in the first frame of an image sequence and subsequently tracked throughout the end of the sequence. The underlying assumption behind template tracking is that the object will not significantly change its appearance throughout the duration of the video. This assumption, however, is not realistic, since an object can undergo several rotations, deformations or partial occlusions, making the template no longer an accurate model of the appearance of the object. A simple but rather naive solution to this problem is to update the template at every frame with a new template corresponding to the tracked position of the object. This approach, however, leads to error accumulation, as small errors are constantly introduced in the location of the template. As a result, the template eventually drifts away from the object and in the most cases gets stuck on the static background of the scene. A compromising solution between these two extremes is to partially update the template, as the weighted average (e.g. 90-10 %) of the current and the initial template, a process often called exponential forgetting. Although this solution offers a somewhat more robust tracking, by allowing the template to adapt, it does not avoid error accumulation, and there is still a high probability that the template will eventually drift away from the object.

Matthews *et al* specifically address the drift problem in [21]. The tracked template is updated at every frame, while maintaining the initial template specified in the first frame. To eliminate drift, the new template is aligned every time to the initial one using a gradient descent rule. This strategy, however, is most suitable for tracking rigid objects (e.g. cars). For objects whose appearance changes over time, the authors adopt an approach of template tracking with Active Appearance Models (AAM). The appearance model and the template are updated at every time instance, leading to more robust tracking algorithm. A similar framework is presented in [22], where a set of adaptive appearance models are used for motion-based tracking. The appearance model used consists of three components. The stable component (S) is used to capture the behavior of temporally stable and slowly varying image observations, the data outlier or 'lost' component (L) is used to capture data outliers due to failures in tracking, occlusion or noise and finally the 'wandering' component (W) is used to model sudden changes in the appearance of the object. The parameters of the model are adjusted online via EM and the system is tested in tracking scenarios where a high degree of partial object occlusion occurs. Finally, in [23] a Support Vector Machine (SVM) is used in order to provide an initial guess for an object position in the first frame. The position of the initial guess in subsequently refined so that a local maximum of the SVM score is achieved. The whole framework is called Support Vector Tracking (SVT) and is implemented in moving vehicle tracking scenarios.

2.2 Human Activity Tracking and Recognition

A major component in human computing research is localization and tracking of the human body, either as a whole or as a part (e.g. head,limbs). Especially for the purposes of scene analysis and activity recognition, body tracking has received a lot of attention in the last few years. Due to its high degree of freedom (usually 28-60), body tracking is inherently a very difficult problem. Because of that, it calls upon sophisticated tracking algorithms, that can address the problem of high dimensionality. Furthermore, large appearance changes, occlusion between body parts, and the absence of typical appearance due to clothing, pose additional problems that need to be dealt with.

In contrast to rigid objects, tracking of articulated objects is inherently a much more difficult problem, mainly due to the high number of degrees of freedom that are involved. Accurate human body tracking, in particular, is an extremely important aspect for human computing applications. A possible strategy for estimating the configuration of articulated objects is sequential search, in which a number of parameters are initially estimated and, assuming that this estimation is correct, the values of several other parameters are determined. For instance, Gavrila and Davis in [24] first locate the torso of the human body and then use this information in order to initialize a search for the limbs. This approach, however, only works for specific views and is very sensitive to self-occlusion that is, occlusion between different body parts. A similar approach is presented in [25], where a particle filtering framework is used for the purposes of hand tracking. For the same purpose, Cipolla *et al* [26] propose a view-based hierarchical probabilistic tracking framework that can deal with changes in view and self occlusions. The system uses edge and color cues in order to estimate the likelihood function of the hand position and configuration and subsequently a Bayesian filtering framework that performs the tracking. In [27] a particle filtering approach is adopted for articulated hand tracking. The tracker is guided by attractors, precollected training samples of possible hand configurations whose observations are known, while the whole process is modeled by a Dynamic Bayesian Network. A Bayesian Network is also adopted in [28] in order to model the existing constraints between the different parts of the human body. These constraints are learned using Gaussian Mixture Models (GMM) and training is done using motion-capture frames of walking data as the ground truth. Observations are based on multi-scale edge and ridge filters while the whole process is assisted with a pooled background model derived by the set of training images. In [29] a Dynamic Markov Network is utilized instead to model the relations between body parts and tracking is done using an sequential Monte Carlo algorithm. A similar approach is presented in [30], where an elastic model is used to represent relations and constraints between the limbs and a Nonparametric Belief Propagation (NBP) algorithm for the purpose of tracking. In [31] a combination of particle filters and Hidden Markov Models (HMM) is used for tracking and recognition respectively, of articulated hand gestures. Appearance-based models are learned for the non-rigid motion of the hand and a filtering method is used for the underlying rigid motion. Both treatments are unified into a single Bayesian framework. A similar approach is implemented in [32], where arm gestures are recognized as a sequence of body poses. The latter are recognized via edge matching and HMMs are used in order to extract the gestures from the pose sequences. HMMs are also used in [33] for recognizing pointing gestures. Skin information is used to localize the hands and the head of the subject in a scene and a multiple hypothesis scheme is used for the tracking. Subsequently, an HMM-based approach is adopted for recognizing the gestures.

Articulated object tracking, and particularly human body tracking suffer from dimensionality issues, an inherent problem whenever there is a large number of degrees of freedom. This fact makes the use of tracking algorithms like particle filters rather impractical. The reason for this is that a very large number of particles is required in order to represent the posterior function in a sufficient way, making this kind of tracking algorithms slow and computationally expensive. The problem becomes even more prominent whenever real-time performance is required, such as in monitoring applications, virtual trainers or augmented reality applications. In order to deal with this issue, a number of different techniques have been proposed, either by constraining the configuration space [24] or by restricting the range of the movements of the subject [34]. These approaches, however, greatly reduce the generality of the implemented trackers, making them impractical in real applications. Eigenspace decomposition [35] and principal component analysis [36] offer an interesting alternative for dimensionality reduction. In [37], a modified particle filtering approach is used in order to reduce the complexity of human body tracking. The main characteristic of the utilized tracker is its ability to avoid local maxima in the tracking by incorporating a search based on simulated annealing, and thus called annealed particle filter. Apart from dimensionality reduction techniques, several researchers have attempted to modify the way classical tracking algorithms work in order to achieve computational efficiency and real-time tracking performance. A simple example are the earlier mentioned kernel-based particle filters [13], [14], [15], [38] or particle filters that use special transformations, as in [16], [17]. These methods attempt to limit the number of required particles for efficient tracking, effectively reducing the computational complexity of their algorithms. Finally, an interesting approach for real-time tracking and recognition of hand actions is presented in [39],[40]. The motion of the hand is extracted using skin cues and is subsequently tracked using the Mean-Shift Tracking scheme of [38]. The spatiotemporal curvatures of the extracted trajectories are used in order to represent the actions performed. The local maxima of these curvatures are view-invariant and are used for image sequence alignment and matching of the actions.

2.3 Unsupervised Representation and Recognition of Actions

Despite their extreme usefulness, tracking methods consist of only a fraction of the methods used for capturing the activity going on in a scene. While trackers mainly concentrate on tracking the state of an object at any time instant, a variety of other methods have been proposed that deal the problem in a more abstract or unsupervised manner [41], [42]. An interesting work is presented in [43], where human actions are treated as three-dimensional shapes in the space-time volume. The method utilizes properties of the solution to the Poisson equation to extract space-time features of the moving human body, such as local space-time saliency, action dynamics, shape structure and orientation. Subsequently, spectral clustering is used in order to group similar actions. In [44], long video sequences are segmented in the time domain by detecting single events in them. The detection is completely unsupervised, since it is done without any prior knowledge of the types of events, their models, or their temporal extent. The method can be used for event-based indexing even when only one short example-clip is available. Unsupervised methods for learning human motion patterns are also presented in [45], [46]. In these methods, the human body is modeled as a triangulated graph. The model is learned in an unsupervised manner from unlabelled data using global and local features, either dynamic or appearance-based. The authors effectively handle occlusion by modeling the missing parts as hidden variables. The parameters of the assumed models are being estimated using EM. Finally, a Hidden Markov Model approach for action recognition is presented in [47]. The activity in a scene is represented by codewords called movelets. Each movelet is a collection of the shape, motion and occlusion of image patches corresponding to the main parts of the body. Recognition is done using HMMs, by estimating the most likely sequence of codewords and the action that took place in a sequence.

2.4 Overview of the Proposed Method

A wide variety of activity recognition methods use edge and color cues [16], [14] or some form of markers [48],[49] in order to assist initialization and the overall operation of tracking or recognition processes. In order to avoid the use of markers, an interesting alternative could be the use of interesting points for tracker initialization. According to Haralick and Shapiro [50] an interesting point is a) distinguishable from its neighbors and b) its position is invariant with respect to the expected geometric transformation and to radiometric distortions. Gilles introduces the notion of saliency in terms of local signal complexity or unpredictability in [51]. Kadir and Brady [52] extend the original Gilles algorithm and estimate the information content of pixels in circular neighborhoods at different scales in terms of the entropy. Local extremes of changes in the entropy across scales are detected and the saliency of each point at a certain scale is defined in terms of the entropy and its rate of change at the scale in question.

In this work, we propose a human action recognition algorithm that is based on the detection and tracking of spatiotemporal features in given image sequences. We do this by extending in the temporal direction the salient feature detector developed in [52]. The detected salient points correspond to peaks in activity variation such as the edges of a moving object. Similar to [43], we treat the action as three-dimensional events, by detecting the salient points in the space-time domain. Contrary to [14], [37], [28] and [29] that use models to represent the human body, we propose an entirely unsupervised method based on the detected salient features in order to represent the moving parts of the body. In this sense, the concept of our method resembles the one in [44], where detection is done without prior knowledge of the types of events, their models, or their temporal extent. Like in [52], we automatically detect the scales at which the entropy achieves local maxima and form spatiotemporal salient regions by clustering spatiotemporal points with similar location and scale. We derive a suitable distance measure between sets of salient regions, which is based on the Chamfer distance, and we optimize this measure with respect to a number of temporal and scaling parameters. In this way we achieve invariance against scaling and we eliminate the temporal differences between the representations. We extend our previous work on salient points presented at [53] by using the detected salient regions in order to initialize a tracking scheme based on the auxiliary particle filter, proposed in [18]. Each image sequence is then represented as a set of short trajectories. The spatiotemporal coordinates of the points that consist the extracted trajectories are appropriately transformed according to the parameters that were estimated in the Chamfer distance optimization step. We use the adaptive background estimation algorithm presented in [54] in order to model the background in the available sequences and to improve the overall quality of the implemented tracking scheme. We use a variant of the Longest Common Subsequence algorithm (LCSS) that was proposed in [55],[56] in order to compare different sets of trajectories. We use Relevance Vector Machines [57] in order to address the classification problem. We propose new kernels for use by the RVM, which are specifically tailored to the proposed short trajectory representation. The basis of these kernels is the modified LCSS distance of the previous step. The novelty of the proposed method lies in the unsupervised nature of representation of the actions. Since we don't use any model, the method can be easily extended and used for a variety of different actions, ranging from full-body actions to single gestures.

The remainder of the paper is organized as follows: In section 3, the spatiotemporal feature detector used is described, along with the proposed space-time warping technique. In section 4, the auxiliary particle filter that was used is briefly analyzed along with the background estimation model that was utilized. In section 5 the proposed kernel-based recognition method is described. In section 6, we present our experimental results, and in section 7, final conclusions are drawn.

3 Spatiotemporal Salient Points

3.1 Spatiotemporal Saliency

Let us denote by $N_c(s, \boldsymbol{v})$ the set of pixels in an image I that belong to a circular neighborhood of radius s, centered at pixel $\boldsymbol{v} = (x, y)$. In [52], in order to detect salient points in static images, Kadir and Brady define a saliency measure $y_D(s, \boldsymbol{v})$ based on measuring changes in the information content of N_c for a set of different circular radiuses (i.e. scales). In order to detect spatiotemporal salient points at peaks of activity variation we extend the Kadir's detector by considering cylindrical spatiotemporal neighborhoods at different spatial radiuses s and temporal depths d. More specifically, let us denote by $N_{cl}(\boldsymbol{s}, \boldsymbol{v})$ the set of pixels in a cylindrical neighborhood of scale $\boldsymbol{s} = (s, d)$ centered at the spatiotemporal point $\boldsymbol{v} = (x, y, t)$ in the given image sequence. At each point $\boldsymbol{v}$ and for each scale $\boldsymbol{s}$ we will define the spatiotemporal saliency $y_D(\boldsymbol{s}, \boldsymbol{v})$ by measuring the changes in the information content within $N_{cl}(\boldsymbol{s}, \boldsymbol{v})$. Since we are interested in activity within an image sequence, we consider as input signal the convolution of the intensity information with a first-order Gaussian derivative filter. Formally, given an image sequence $I_0(x, y, t)$ and a filter G_t, the input signal that we use is defined as:

$$I(x, y, t) = G_t * I_0(x, y, t)\,. \tag{1}$$

For each point $\boldsymbol{v}$ in the image sequence, we calculate the Shannon entropy of the signal histogram in a cylindrical neighborhood $N_s(\boldsymbol{s}, \boldsymbol{v})$ around it. That is,

$$H_D(s, d, \boldsymbol{v}) = -\sum_{q \in D} p(q, s, d, \boldsymbol{v}) \log p(q, s, d, \boldsymbol{v}) \,, \tag{2}$$

The set of scales at which the entropy is peaked is given by:

$$\begin{aligned} \hat{S}_p = \{(s, d) : & H_D(s-1, d, \boldsymbol{v}) < H_D(s, d, \boldsymbol{v}) > H_D(s+1, d, \boldsymbol{v}) \\ & \wedge H_D(s, d-1, \boldsymbol{v}) < H_D(s, d, \boldsymbol{v}) > H_D(s, d+1, \boldsymbol{v})\} \end{aligned} \tag{3}$$

The saliency measure at the candidate scales is given by:

$$y_D(s, d, \boldsymbol{v}) = H_D(s, d, \boldsymbol{v}) W_D(s, d, \boldsymbol{v}), \quad \forall\, (s, d) \in \hat{S}_p \,, \tag{4}$$

The first term of eq. 4 is a measure of the variation in the information content of the signal. The weighting function $W_D(s, \boldsymbol{v})$ is a measure of how prominent the local maximum is at s, and is given by:

$$\begin{aligned} W_D(s, d, \boldsymbol{v}) = & \frac{s^2}{2s-1} \sum_{q \in D} |p(q, s, d, \boldsymbol{v}) - p(q, s-1, d, \boldsymbol{v})| \\ & + d \sum_{q \in D} |p(q, s, d, \boldsymbol{v}) - p(q, s, d-1, \boldsymbol{v})|, \forall\, (s, d) \in \hat{S}_p \,, \end{aligned} \tag{5}$$

where the values in front of each summation in the right part of eq. 5 are normalization factors. When a peak in the entropy for a specific scale is distinct, then the corresponding pixel probability density functions at the neighboring scales will differ substantially, giving a large value to the summations of eq. 5 and thus, to the corresponding weight value assigned. On the contrary, when the peak is smoother, then the summations in eq. 5 will have a smaller value. Let us note that we considered cylindrical neighborhoods for simplicity reasons. However, more complicated shapes, such as elliptical neighborhoods at different orientations and with different axes ratios could be considered.

In Fig. 1(a), a single frame from a sample image sequence is presented, where the subject is raising its right hand. By selecting as origin the center pixel of the drawn white circle, we apply a number of cylindrical neighborhoods of various scales in the sequence and we calculate the corresponding entropy values. The result is shown in Fig. 1(b), where the various entropy values are plotted with respect to the radiuses and depths of the corresponding cylindrical neighborhoods. The scale which corresponds to the distinct peak of the plot is considered candidate salient scale, and is assigned a saliency value, according to eq. 4.

3.2 Salient Regions

The analysis of the previous section leads to a set of candidate spatiotemporal salient points $S = \{(\boldsymbol{s}_i, \boldsymbol{v}_i, y_{D,i})\}$, where $\boldsymbol{v}_i = (x, y, t)$, $\boldsymbol{s}_i$ and $y_{D,i}$ are respectively, the position vector, the scale and the saliency value of the feature point with index i. In order to achieve robustness against noise we follow a similar approach as that in [52] and develop a clustering algorithm, which we apply to

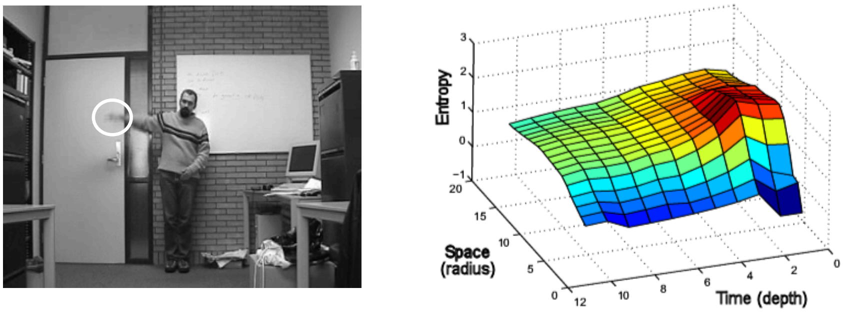

(a) (b)

Fig. 1. (a) Single frame from a sample image sequence where the subject is raising its right hand and (b) the corresponding entropy plot as a function of the spatial radius and temporal depth of all the applied cylindrical neighborhoods. The origin of all the applied cylindrical neighborhoods is the center of the white circle in (a).

the detected salient points. By this we define salient regions instead of salient points, the location of which should be more stable than the individual salient points, since noise is unlikely to affect all of the points within the region in the same way. The proposed algorithm removes salient points with low saliency and creates clusters that are a) well localized in space, time and scale, b) sufficiently salient and c) sufficiently distant from each other. The steps of the proposed algorithm can be summarized as follows:

1. Derive a new set S_T from S by applying a global threshold T to the saliency of the points that consist S. Thresholding removes salient points with low saliency, that is,
$$S_T = \{(\boldsymbol{s}_i, \boldsymbol{v}_i, y_{D,i}) : y_{D,i} > T\} \,. \tag{6}$$
2. Select the point i in S_T with the highest saliency value and use it as a seed to initialize a salient region R_k. Add nearby points j to the region R_k as long as the intra-cluster variance does not exceed a threshold T_V. That is, as long as
$$\frac{1}{|R_k|} \sum_{j \in R_k} c_j^2 < T_V \,, \tag{7}$$
where R_k is the set of the points in the current region k and c_j is the Euclidean distance of the jth point from the seed point i.
3. If the overall saliency of the region R_k is lower than a saliency threshold T_S,
$$\sum_{j \in R_k} y_{D,j} \leq T_S \,, \tag{8}$$
discard the points in the region back to the initial set of points and continue from step 2 with the next highest salient point. Otherwise, calculate the Euclidean distance of the center of region R_k from the center of salient regions already defined, that is, from salient regions $R_{k'}, k' < k$.

4. If the distance is lower than the average scale of R_k, discard the points in R_k back to the initial set of points, and continue with the next highest salient point. Otherwise, accept R_k as a new cluster and store it as the mean scale and spatial location of the points in it.
5. Form a new set S_T consisting of the remaining salient points, increase the cluster index k and continue from step 2 with the next highest salient point.

By setting the threshold T_V in step 2, we define clusters that have local support and are well localized in space and time. In addition, we want to take the saliency of the points into consideration such that the overall saliency of the region is sufficient. We do this in step 3, by setting a saliency threshold, T_S. Finally, the purpose of step 4 is to accept clusters that are sufficiently distant from each other. To summarize, a new cluster is accepted only if it has sufficient local support, its overall saliency value is above the saliency threshold, and it is sufficiently distant in terms of Euclidean distance from already existing clusters.

3.3 Space-Time Warping

There is a large amount of variability between feature sets due to differences in the execution speed of the corresponding actions. Furthermore, we need to compensate for possible shifting of the representations forward or backward in time, caused by imprecise segmentation of the corresponding actions. To cope with both these issues, we propose a linear space-time warping technique with which we model variations in time using a time-scaling parameter a and a time-shifting parameter b. In addition, in order to achieve invariance against scaling, we introduce a scaling parameter c in the proposed warping technique. To accommodate this procedure, we propose the Chamfer distance as an appropriate distance measure, in order to cope with unequal number of features between different sets of salient points. More specifically, for two feature sets $F = \{(x_i, y_i, t_i), 1 \le i \le M\}$ and $F' = \{(x'_j, y'_j, t'_j), 1 \le j \le M'\}$ consisting of an M and M' number of features, respectively, the Chamfer distance of the set F from the set F' is defined as follows:

$$D(F, F') = \frac{1}{M} \sum_{i=1}^{M} \min_{j=1}^{M'} \sqrt{(x'_j - x_i)^2 + (y'_j - y_i)^2 + (t'_j - t_i)^2}\,. \tag{9}$$

From eq. 9 it is obvious that the selected distance measure is not symmetrical, as $D(F, F') \neq D(F', F)$. For recognition purposes, it is desirable to select a distance measure that is symmetrical. A measure that satisfies this requirement is the average of $D(F, F')$ and $D(F', F)$, that is,

$$D_c(F, F') = \frac{1}{2}(D(F, F') + D(F', F))\,. \tag{10}$$

Let us denote by $F_w = \{(cx_i, cy_i, at_i - b), 1 \le i \le M\}$ the feature set F with respect to feature set F'. Then, the distance between F' and F_w is given by eq. 9 as:

$$D(F_w, F') = \frac{1}{M} \sum_{i=1}^{M} \min_{j=1}^{M'} \sqrt{(x'_j - cx_i)^2 + (y'_j - cy_i)^2 + (t'_j - at_i + b)^2}\,. \tag{11}$$

Similarly, the feature set F' with respect to feature set F can be represented as $F'_w = \{(\frac{1}{c}x'_j, \frac{1}{c}y'_j, \frac{1}{a}t'_j + b), 1 \leq j \leq M'\}$ and their distance as:

$$D(F'_w, F) = \frac{1}{M'} \sum_{j=1}^{M'} \min_{i=1}^{M} \sqrt{(x_i - \frac{1}{c}x'_j)^2 + (y_i - \frac{1}{c}y'_j)^2 + (t_i - \frac{1}{a}t'_j - b)^2} \,. \tag{12}$$

The distance to be optimized follows from the substitution of eq. 11 and eq. 12 to eq. 10. We follow an iterative gradient descent approach for the adjustment of the a, b and c parameters. The update rules are given by:

$$a^{n+1} = a^n - \lambda_1 \frac{\partial D_c}{\partial a^n}, \tag{13}$$

$$b^{n+1} = b^n - \lambda_2 \frac{\partial D_c}{\partial b^n}, \tag{14}$$

$$c^{n+1} = c^n - \lambda_3 \frac{\partial D_c}{\partial c^n}\,, \tag{15}$$

where $\lambda_1, \lambda_2, \lambda_3$ are the learning rates and n is the iteration index. The algorithm iteratively adjusts the values of a, b and c towards the minimization of the Chamfer distance between the two feature sets, given by eq. 10. The iterative procedure stops when the values of a, b and c do not change significantly or after a fixed number of iterations.

4 Tracking

4.1 Auxiliary Particle Filtering

Recently, particle filtering tracking schemes [10], [18], have been successfully used [58], [59], [19] in order to track the state of a temporal event given a set of noisy observations. Its ability to maintain simultaneously multiple solutions, called particles, makes it particularly attractive when the noise in the observations is not Gaussian and makes it robust to missing or inaccurate data.

The particle filtering tracking scheme described in this section is initialized at the spatiotemporal salient points that are detected using the procedure of section 3. Let c denote the template that contains the color information in a rectangular window centered at each detected salient point and α denote the unknown location of the facial feature at the current time instant. Furthermore, let us denote by $Y = \{y^1, \ldots, y^-, y\}$ the observations up to the current time instant. The main idea of the particle filtering is to maintain a particle based representation of the a posteriori probability $p(\alpha|Y)$ of the state α given all the observations Y up to the current time instance. The distribution $p(\alpha|Y)$ is represented by a set of pairs (s_k, π_k) such that if s_k is chosen with probability equal to π_k, then it is as if s_k was drawn from $p(\alpha|Y)$. Our knowledge about the a posteriori probability is updated in a recursive way. Suppose that we have a particle based representation of the density $p(\alpha^-|Y^-)$, that is we have a collection of K particles and their corresponding weights (i.e. (s_k^-, π_k^-)). Then, the Auxiliary Particle Filtering can be summarized as follows:

1. Propagate all particles s_k^- via the transition probability $p(\alpha|\alpha^-)$ in order to arrive at a collection of K particles μ_k.
2. Evaluate the likelihood associated with each particle μ_k, that is let $\lambda_k = p(y|\mu_k; c)$.
   For the definition of $p(y|\mu_k; c)$ we use, in this paper, the observation model described in [19].
3. Draw K particles s_k^- from the probability density that is represented by the collection $(s_k^-, \lambda_k \pi_k^-)$. In this way, the auxiliary particle filter favors particles with high λ_k, that is particles which, when propagated with the transition density, end up at areas with high likelihood.
4. Propagate each particle s_k^- with the transition probability $p(\alpha|\alpha^-)$ in order to arrive at a collection of K particles $s_k{}'$.
5. Assign a weight $\pi_k{}'$ to each particle as follows,

$$w_k{}' = \frac{p(y|s_k{}'; c)}{\lambda_k}, \quad \pi_k{}' = \frac{w_k{}'}{\sum_j w_j} \tag{16}$$

   This results in a collection of K particles and their corresponding weights (i.e. $\{(s_k{}', \pi_k{}')\}$) which is an approximation of the density $p(\alpha|Y)$.

4.2 Online Background Estimation

The particle filtering tracking scheme described in the previous section is initialized at the spatiotemporal salient points that are detected using the procedure described in section 3. As indicated from eq. 1, the input signal that is used is the convolution of the original image sequence with a Gaussian derivative filter along the temporal dimension. The result of this is that the detected salient points are localized on the edges of the moving objects existing in the scene, rather than on the objects themselves. This fact may deteriorate the output of the tracker used, since the patches of the sequence that are being tracked also include a considerable portion of the scene's background. For this reason, we implement the adaptive background estimation algorithm described in [54], in order to determine which pixels belong to the foreground and which ones to the background. According to this algorithm, the values of a particular pixel over time are considered as a temporal process. At each time t, what is known about a particular pixel (x_0, y_0) is its history:

$$\{X_1, \ldots, X_t\} = \{I(x_0, y_0, i) : 1 \leq i \leq t\}, \tag{17}$$

where I is the image sequence. The recent history of each pixel is modeled by a mixture of K Gaussian distributions. The probability of observing the current pixel value is given by:

$$P(X_t) = \sum_{i=1}^{K} w_{i,t} \cdot \eta(X_t, \mu_{i,t}, \Sigma_{i,t}), \tag{18}$$

where K is the number of distributions, $w_{i,t}$ is an estimate of the weight of the i_{th} Gaussian in the mixture at time t, $\mu_{i,t}$ is the mean value of the i_{th} Gaussian in the mixture at time t, $\Sigma_{i,t}$ is the covariance matrix of the i_{th} Gaussian in the mixture at time t, and η is a Gaussian probability density function. K was set to 3, and the covariance matrix Σ is assumed to be diagonal, meaning that the RGB values of the pixels are assumed to be uncorrelated.

The parameters of each Gaussian mixture were initially estimated using the Expectation-Maximization (EM) algorithm and by using a small portion of the available data (i.e. the first few frames of the image sequence). Subsequently at each new frame t we follow an update procedure similar to the one of [54]. Every new pixel value X_t is checked against the existing K distributions until a match is found. A match is defined if the current pixel is within 3 standard deviations of a distribution. In case a match is found the parameters of the Gaussians are updated. If none of the K distributions match the current pixel value, the least probable distribution is replaced with a distribution with the current value as its mean value, an initially high variance, and low prior weight.

At each iteration of the particle filtering tracking scheme of section 4.1, every new particle is evaluated based on an invariant colour distance between the initial template (centered at the initializing spatiotemporal salient point) and the block that corresponds to the particle that is being evaluated. In order to take the estimated background model into account, we add an additional cost in the evaluation process of each new particle. The additional cost for every pixel is equal to the probability that the pixel belongs to the current background model, that is,

$$C_{i,j,t} = \sum_{i=1}^{K} w_{i,j} \eta(X_{j,t}, \mu_{i,j,t}, \Sigma_{i,j,t}), \tag{19}$$

where K is the number of distributions, $w_{i,j,t}$ is an estimate of the weight of the i_{th} Gaussian in the mixture for the pixel j at time t, $\mu_{i,j,t}$ is the mean value

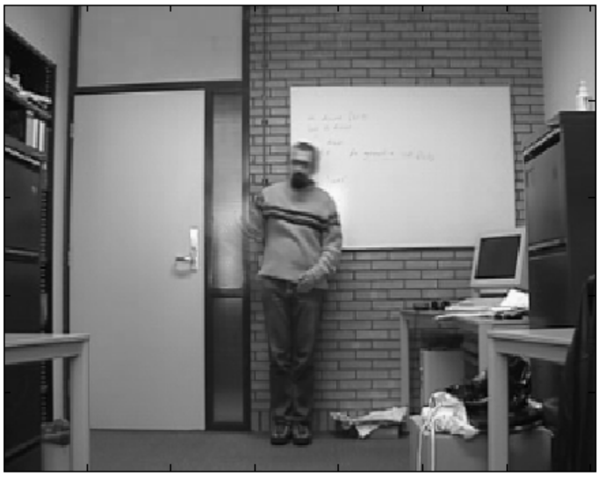

Fig. 2. Initial estimation of the background for an action where the subject is just raising its right hand

of the i_{th} Gaussian in the mixture for the pixel j at time t and $\Sigma_{i,j,t}$ is the covariance matrix of the i_{th} Gaussian in the mixture for pixel j at time t.

If a pixel in the block belongs to the background, then eq. 19 will assign a large cost to that pixel, since the resulting probability will be high. If most pixels in the block belong to the background, then the additional cost to that block will also be large and consequently, a smaller weight will be assigned to it by the particle filter. In this way, the tracking scheme favors blocks that contain larger number of foreground pixels and assigns larger weights to the corresponding particles.

In Fig. 2 the initial background model that was estimated for an action where the subject is raising its right hand is presented. As can be seen from the figure, parts of the body that do not present significant motion are also considered part of the background. On the other hand, fast moving parts (e.g. right hand) are considered to belong to the foreground and are not included in the estimation.

5 Recognition

5.1 Longest Common Subsequence (LCSS) Algorithm

Using the analysis of the previous sections, we represent a given image sequence by a set of short trajectories, where each trajectory is initialized at a point which is considered salient both in space and time. Formally, an image sequence is represented by a set of trajectories $\{A_i\}, i = 1 \ldots K$, where K is the number of trajectories that consist the set. Each trajectory is defined as $A_i = ((t_{i,n}, x_{i,n}, y_{i,n}), \ldots)$, $n = 1 \ldots N$, where $t_{i,n}, x_{i,n}, y_{i,n}$ are spatiotemporal coordinates and N is the number of samples that consist A_i. Let us define another trajectory set $\{B_j\}$, $j = 1 \ldots L$ representing a different image sequence. Similar to $\{A_i\}$, the trajectories in $\{B_j\}$ are defined as $B_j = ((t_{j,m}, x_{j,m}, y_{j,m}), \ldots)$, $m = 1 \ldots M$, where M is the number of individual trajectories that consist $\{B_j\}$. We use a variant of the LCSS algorithm presented at [55], [56] in order to compare the two sets. Before we proceed with the comparison, we align the two sets in space and time using the a, b and c parameters that were computed using the procedure of section 3.3. Let us define the function $Head(A_i) = ((t_{i,n}, x_{i,n}, y_{i,n})), n = 1 \ldots N-1$, that is, the individual trajectory A_i reduced by one sample. Then, according to the LCSS algorithm, the distance between individual trajectories A_i and B_j is given by:

$$d_L(A_i, B_j) = \begin{cases} 0, \quad if\ A_i\ or\ B_j\ is\ empty \\ \\ d_e((t_{i,n}, x_{i,n}, y_{i,n}), (t_{j,m}, x_{j,m}, y_{j,m})) \\ +d_L(Head(A_i), Head(B_j)), \\ if\ \ |t_{i,n} - t_{j,m}| < \delta\ and\ \ |x_{i,n} - x_{j,m}| < \varepsilon \\ and\ \ |y_{i,n} - y_{j,m}| < \varepsilon \\ \\ \max(d_L(Head(A_i), B_j), d_L(A_i, Head(B_j))) + p, \\ otherwise \end{cases}, \qquad (20)$$

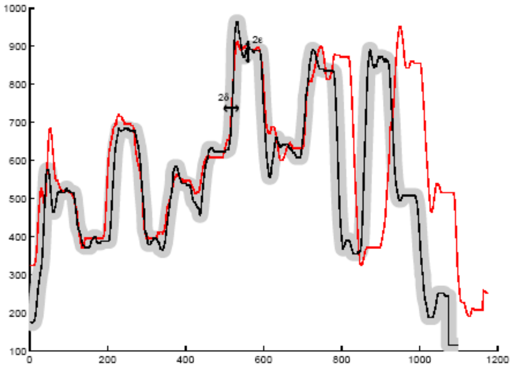

Fig. 3. The notion of the LCSS matching within a region of δ and ϵ of a trajectory

where d_e is the Euclidean distance, δ controls how far in time we can go in order to match a given point from one trajectory to a point in another trajectory, ϵ is the matching threshold and p is a penalty cost in case of mismatch. The notion of the LCSS distance of eq. 20 is depicted in Fig. 3.

Subsequently, the distance between sets $\{A_i\}$ and $\{B_j\}$is defined as follows:

$$D_L(\{A_i\},\{B_j\}) = \frac{1}{K}\sum_i \min_j d_L(A_i, B_j) + \frac{1}{L}\sum_j \min_i d_L(B_j, A_i), \tag{21}$$

that is, the average over the set of the minimum distances, as they have been defined in eq. 20, between the K trajectories of set $\{A_i\}$ and the L trajectories of set $\{B_j\}$.

5.2 Relevance Vector Machine Classifier

We propose a classification scheme based on Relevance Vector Machines [57] in order to classify given examples of human actions. A Relevance Vector Machine (RVM) is a probabilistic sparse kernel model identical in functional form to the Support Vector Machines (SVM). In their simplest form, Relevance Vector Machines attempt to find a hyperplane defined as a weighted combination of a few Relevance Vectors that separate samples of two different classes. In contrast to SVM, predictions in RVM are probabilistic. Given a dataset of N input-target pairs $\{(F_n, l_n), 1 \leq n \leq N\}$, an RVM learns functional mappings of the form:

$$y(F) = \sum_{n=1}^{N} w_n K(F, F_n) + w_0\,, \tag{22}$$

where $\{w_n\}$ are the model weights and $K(.,.)$ is a Kernel function. Gaussian or Radial Basis Functions have been extensively used as kernels in RVM. In our case, we use as a kernel a Gaussian Radial Basis Function defined by the distance measure of eq. 21. That is,

$$K(F, F_n) = e^{-\frac{D_L(F,F_n)^2}{2\eta}}\,, \tag{23}$$

where η is the Kernel width. RVM performs classification by predicting the posterior probability of class membership given the input F. The posterior is given by wrapping eq. 22 in a sigmoid function, that is:

$$p(l|F) = \frac{1}{1 + e^{-y(F)}} \tag{24}$$

In the two class problem, a sample F is classified to the class $l \in [0, 1]$, that maximizes the conditional probability $p(l|F)$. For L different classes, L different classifiers are trained and a given example F is classified to the class for which the conditional distribution $p_i(l|F)$,$1 \leq i \leq L$ is maximized, that is:

$$Class(F) = \arg\max_i (p_i(l|F))\,. \tag{25}$$

6 Experimental Results

For the evaluation of the proposed method, we use aerobic exercises as a test domain. Our dataset consists of 12 different aerobic exercises, performed by amateurs, that have seen a video with an instructor performing the same set of exercises. Each exercise is performed twice by four different subjects, leading to a set of 96 corresponding feature sets.

In order to illustrate the ability of the proposed method to extract the kind of motion performed, we present in Fig. 4 the trajectories that were extracted

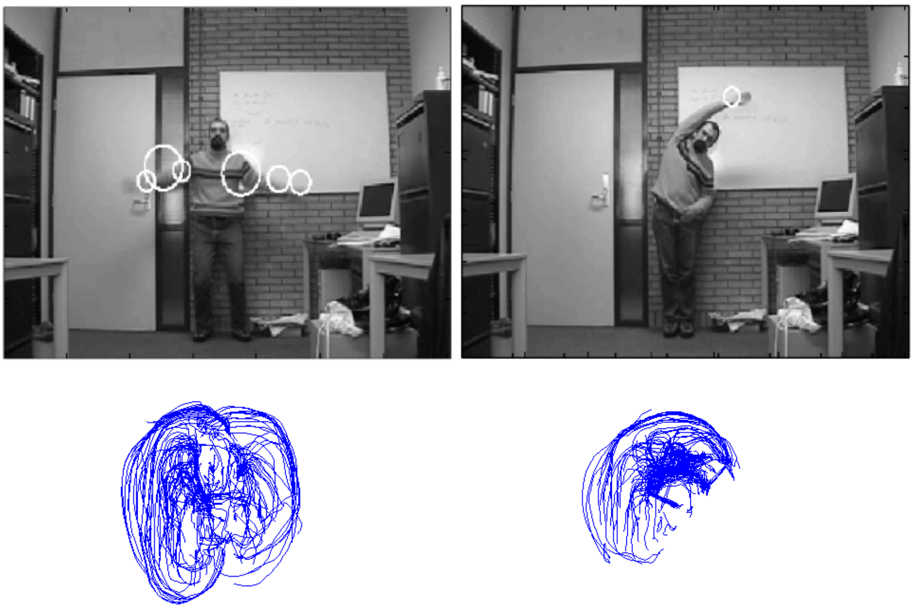

Fig. 4. Extracted trajectories for two different actions

Table 1. Recall and Precision rates for the kNN and RVM classifiers

Class Labels	**1**	**2**	**3**	**4**	**5**	**6**
RVM Recall	1	1	1	1	0.5	0.5
RVM Precision	1	1	1	1	0.44	0.4
Class Labels	**7**	**8**	**9**	**10**	**11**	**12**
RVM Recall	1	0.88	0.63	0.63	0.88	1
RVM Precision	1	1	0.63	0.83	0.88	1

Table 2. RVM Confusion Matrix

Class labels	**1**	**2**	**3**	**4**	**5**	**6**	**7**	**8**	**9**	**10**	**11**	**12**	**Total**
1	**8**	0	0	0	0	0	0	0	0	0	0	0	8
2	0	**8**	0	0	0	0	0	0	0	0	0	0	8
3	0	0	**8**	0	0	0	0	0	0	0	0	0	8
4	0	0	0	**8**	0	0	0	0	0	0	0	0	8
5	0	0	0	0	**4**	5	0	0	0	0	0	0	9
6	0	0	0	0	4	**3**	0	0	3	0	0	0	10
7	0	0	0	0	0	0	**8**	0	0	0	0	0	8
8	0	0	0	0	0	0	0	**7**	0	0	0	0	7
9	0	0	0	0	0	0	0	1	**5**	2	0	0	8
10	0	0	0	0	0	0	0	0	0	**5**	1	0	6
11	0	0	0	0	0	0	0	0	0	1	**7**	0	8
12	0	0	0	0	0	0	0	0	0	0	0	**8**	8
Total	8	8	8	8	8	8	8	8	8	8	8	8	8

from two different actions along with a snapshot of the corresponding actions. The salient points that are visible in the upper part of the figure were used in order to extract some of the trajectories presented in the lower part of the same Figure. Furthermore, the extracted trajectory set seems to correctly capture the pattern of the motion performed. This can easily be observed from the arch-like trajectories of the lower part of the figure, which correspond to the motion of the subjects' hands.

In order to classify a test example using the Relevance Vector Machines, we constructed 12 different classifiers, one for each class, and we calculated for each test example F the conditional probability $p_i(l|F), 1 \leq i \leq 12$. Each example was assigned to the class for which the corresponding classifier provided the maximum conditional probability, as depicted in eq. 25. Note that for estimating each of the $p_i(l|F)$, an RVM is trained by leaving out the example F as well as all other instances of the same exercise that were performed by the subject from F. The corresponding recall and precision rates, calculated as an average of all test trials, are given in Table 1. The total recognition rate is equal to 80.61%, which is a relatively good performance, given the small number of examples with respect to the number of classes, and the fact that the subjects were not trained. In Table 2 the confusion matrix generated by the RVM classifier is also given.

The confusion matrix in Table 2 conceals the fact that for some of the misclassified examples the probability assigned by the RVM classifier to the correct matching move might be very close to the probability assigned to the move actually selected by the classifier. We used the average ranking percentile in order to extract this kind of information and to measure the overall matching quality of our proposed algorithm. Let us denote with r^{F_n} the position of the correct match for the test example $F_n, n = 1 \ldots N_2$, in the ordered list of N_1 match values. Rank r^{F_n} ranges from $r = 1$ for a perfect match to $r = N_1$ for the worst possible match. Then, the average ranking percentile is calculated as follows:

$$\overline{r} = \left(\frac{1}{N_2} \sum_{n=1}^{N_2} \frac{N_1 - r^{F_n}}{N_1 - 1} \right) 100\%. \tag{26}$$

Since our dataset consists of 96 test image sequences divided in 12 separate classes, it follows that $N_1 = 12$ and $N_2 = 96$. Each of the 12 match values are provided for each example by the 12 trained RVM classifiers. The average ranking percentile for the RVM classifier is 94.5%. Its high value shows that for the majority of the missclassified examples, the correct matches are located in the first positions in the ordered list of match values.

7 Conclusions

In this work, previous work on spatiotemporal saliency was enhanced in order to extract a number of short trajectories from given image sequences. Each detected spatiotemporal point was used in order to initialize a tracker based on auxiliary particle filtering. A background estimation model was also implemented and incorporated into the particle evaluation process, in order to deal with inadequate localization of the initialization points and to improve, thus, the performance of the tracker. A variant of the LCSS algorithm was used in order to compare different sets of trajectories. The derived LCSS distance was used in order to define a kernel for the RVM classifier that was used for recognition. We have illustrated the efficiency of our representation in recognizing human actions using as a test domain aerobic exercises. Finally, we presented results on real image sequences that illustrate the consistency in the spatiotemporal localization and scale selection of the proposed method.

Acknowledgements

This work has been partially supported by the Dutch-French Van Gogh program (project VGP-62-604) and the work of A. Oikonomopoulos has been supported by the Greek State Scholarship Foundation (IKY). The data set was collected while I. Patras was with the ISIS group at the University of Amsterdam.

References

1. Pantic, M., Pentland, A., Nijholt, A., Huang, T.: Human computing and machine understanding of human behavior: A survey. International Conference on Multimodal Interfaces (2006)
2. Wang, J.J., Singh, S.: Video analysis of human dynamics - A survey. Real Time Imaging **9** (2003) 321 – 346
3. Wang, L., Hu, W., Tan, T.: Recent Developments in Human Motion Analysis. Pattern Recognition **36** (2003) 585 – 601

4. Bar-Shalom, Y., Fortmann, T.: Tracking and Data Association. Academic Press (1988)
5. Julier, S., Uhlmann, J.: Unscented filtering and nonlinear estimation. Proceedings of the IEEE **92** (2004) 401–422
6. Wu, Y., Hu, D., Wu, M., Hu, X.: Unscented kalman filtering for additive noise case: Augmented versus nonaugmented. IEEE Signal Processing Letters **12** (2005) 357–360
7. LaViola, J.: A comparison of unscented and extended Kalman filtering for estimating quaternion motion. Proceedings of the American Control Conference **3** (2003) 2435 – 2440
8. Zhang, Y., Ji, Q.: Active and dynamic information fusion for facial expression understanding from image sequences. IEEE Trans. Pattern Analysis and Machine Intelligence **27** (2005) 699 – 714
9. Gu, H., Ji, Q.: Information extraction from image sequences of real-world facial expressions. Machine Vision and Applications **16** (2005) 105 – 115
10. Isard, M., Blake, A.: Condensation conditional density propagation for visual tracking. International Journal of Computer Vision **29** (1998) 5 – 28
11. Isard, M., Blake, A.: Icondensation: Unifying low-level and high-level tracking in a stochastic framework. European Conference on Computer Vision **29** (1998) 893 – 908
12. Lichtenauer, J., Hendriks, M.R.E.: Influence of the observation likelihood function on particle filtering performance in tracking applications. Automatic Face and Gesture Recognition (2004) 767– 772
13. Chang, C., Ansari, R., Khokhar, A.: Multiple object tracking with kernel particle filter. Proceedings, IEEE Conference on Computer Vision and Pattern Recognition **1** (2005) 566– 573
14. Schmidt, J., Fritsch, J., Kwolek, B.: Kernel particle filter for real-time 3D body tracking in monocular color images. Automatic Face and Gesture Recognition (2006) 567– 572
15. Comaniciu, D., Ramesh, V., Meer, P.: Kernel-Based Object Tracking. IEEE Trans. Pattern Analysis and Machine Intelligence **25** (2003) 564–577
16. Yang, C., Duraiswami, R., Davis, L.: Fast multiple object tracking via a hierarchical particle filter. Proc. IEEE Int. Conf. Computer Vision **1** (2005) 212– 219
17. Shan, C., Wei, Y., Tan, T., Ojardias, F.: Real time hand tracking by combining particle filtering and mean shift. Automatic Face and Gesture Recognition **1** (2004) 669– 674
18. Pitt, M., Shephard, N.: Filtering via simulation: auxiliary particle filtering. J. American Statistical Association **94** (1999) 590 –
19. Patras, I., Pantic, M.: Tracking deformable motion. IEEE International Conference on Systems, Man and Cybernetics (2005) 1066 – 1071
20. Patras, I., Pantic, M.: Particle filtering with factorized likelihoods for tracking facial features. Automatic Face and Gesture Recognition (2004) 97 – 102
21. Matthews, I., Ishikawa, T., Baker, S.: The template update problem. In Proceedings of the British Machine Vision Conference. (2003)
22. Jepson, A., Fleet, D., El-Maraghi, T.: Robust Online Appearance Models for Visual Tracking. IEEE Trans. Pattern Analysis and Machine Intelligence **25** (2003) 1296–1311
23. Avidan, S.: Support Vector Tracking. IEEE Trans. Pattern Analysis and Machine Intelligence **26** (2004) 1064–1072

24. Gavrila, D., Davis, L.: 3-D Model-Based Tracking of Humans in Action: A Multi-view Approach. Proceedings, IEEE Conference on Computer Vision and Pattern Recognition (1996) 73–80
25. MacCormick, J., Isard, M.: Partitioned Sampling, Articulated Objects and Interface-Quality Hand Tracking. Proceedings, IEEE Conference on Computer Vision and Pattern Recognition (2000) 3–19
26. Stenger, B., Thayananthan, A., Torr, P., Cipolla, R.: Model-Based Hand Tracking Using a Hierarchical Bayesian Filter. IEEE Trans. Pattern Analysis and Machine Intelligence **28** (2006) 1372–1384
27. Chang, W., Chen, C., Hung, Y.: Appearance-guided particle filtering for articulated hand tracking. Proceedings, IEEE Conference on Computer Vision and Pattern Recognition **1** (2005) 235– 242
28. Sigal, L., Bhatia, S., Roth, S., Black, M., M. Isard, M.: Tracking loose-limbed people. Proceedings, IEEE Conference on Computer Vision and Pattern Recognition **1** (2004) 421–428
29. Wu, Y., Hua, G., Yu, T.: Tracking articulated body by dynamic Markov network. Proc. IEEE Int. Conf. Computer Vision **2** (2003) 1094– 1101
30. Han, T., Ning, H., Huang, T.: Efficient Nonparametric Belief Propagation with Application to Articulated Body Tracking. Proceedings, IEEE Conference on Computer Vision and Pattern Recognition **1** (2006) 214– 221
31. Fei, H., Reid, I.: Probabilistic Tracking and Recognition of Non-Rigid Hand Motion. Int. Workshop on Analysis and Modeling of Faces and Gestures (2003) 60–67
32. Elgammal, A., Shet, V., Yacoob, Y., Davis, L.: Exemplar-based tracking and recognition of arm gestures. Proc. Int. Symposium on Image and Signal Processing and Analysis **2** (2003) 656–661
33. Nickel, K., Seemann, E., Stiefelhagen, R.: 3D-Tracking of Head and Hand for Pointing Gesture Recognition in a Human-Robot Interaction Scenario. Automatic Face and Gesture Recognition (2004) 565–570
34. Deutscher, J., Blake, A., North, B., Bascle, B.: Tracking through Singularities and discontinuities by random sampling. Proc. IEEE Int. Conf. Computer Vision **2** (1999) 1144–1149
35. Black, M., Jepson, A.: Eigentracking: Robust matching and tracking of articulated objects using a view-based representation. International Journal of Computer Vision **26** (1998) 63–84
36. Kato, M., Y.W.Chen, G.Xu: Articulated Hand Tracking by PCA-ICA Approach. Automatic Face and Gesture Recognition (2006) 329– 334
37. Deutscher, J., Blake, A., Reid, I.: Articulated body motion capture by annealed particle filtering. Proceedings, IEEE Conference on Computer Vision and Pattern Recognition **2** (2000) 126–133
38. Comaniciu, D., Ramesh, V., Meer, P.: Real-Time Tracking of non-rigid objects using mean-shift. Proceedings, IEEE Conference on Computer Vision and Pattern Recognition **2** (2000) 142–149
39. Rao, C., Yilmaz, A., Shah, M.: View-invariant representation and recognition of actions. International Journal of Computer Vision **50** (2002) 203–226
40. Rao, C., Gritai, A., Shah, M., Syeda-Mahmood, T.: View-invariant alignment and matching of video sequences. Proc. IEEE Int. Conf. Computer Vision **2** (2003) 939–945
41. Gavrila, D.: The Visual Analysis of Human Movement: A Review. Comp. Vision, and Image Understanding **73** (1999) 82–92
42. Aggarwal, J., Cai, Q.: Human Motion Analysis: A Review. Comp. Vision, and Image Understanding **73** (1999) 428–440

43. Blank, M., Gorelick, L., Shechtman, E., Irani, M., Basri, R.: Actions as space-time shapes. Proc. IEEE Int. Conf. Computer Vision **2** (2005) 1395 – 1402
44. Zelnik-Manor, L., Irani, M.: Event-based analysis of video. Proceedings, IEEE Conference on Computer Vision and Pattern Recognition **2** (2001) 123 – 130
45. Song, Y., Goncalves, L., Perona, P.: Unsupervised Learning of Human Motion. IEEE Trans. Pattern Analysis and Machine Intelligence **25** (2003) 814–827
46. Fanti, C., Zelnik-Manor, L., Perona, P.: Hybrid Models for Human Motion Recognition. Proceedings, IEEE Conference on Computer Vision and Pattern Recognition **1** (2005) 1166–1173
47. Feng, X., Perona, P.: Human action recognition by sequence of movelet codewords. Proc. Int. Symposium on 3D Data Processing Visualization and Transmission (2002) 105–115
48. Figueroa, P., Leitey, N., Barros, R., Brenzikofer, R.: Tracking markers for human motion analysis. Proc. of IX European Signal Processing Conf., Rhodes, Greece (1998) 941 – 944
49. Moeslund, T., Nrgaard, L.: A brief overview of hand gestures used in wearable human computer interfaces. Technical Report CVMT 03-02, ISSN 1601-3646 (2003)
50. Haralick, R., Shapiro, L.: Computer and Robot Vision II. Addison-Wesley (1993) Reading, MA.
51. Gilles, S.: Robust Description and Matching of Images. PhD thesis, University of Oxford (1998)
52. Kadir, T., Brady, M.: Scale saliency: a novel approach to salient feature and scale selection. International Conference on Visual Information Engineering (2000) 25 – 28
53. Oikonomopoulos, A., Patras, I., Pantic, M.: Spatiotemporal Salient Points for Visual Recognition of Human Actions. IEEE Trans. Systems, Man and Cybernetics Part B **36** (2005) 710 – 719
54. Stauffer, C.: Adaptive background mixture models for real-time tracking. Proceedings, IEEE Conference on Computer Vision and Pattern Recognition (1999) 246 – 252
55. Vlachos, M., Kollios, G., Gunopulos, D.: Discovering similar multidimensional trajectories. Proc. International Conference on Data Engineering (2002) 673 – 684
56. Buzan, D., Sclaroff, S., Kollios, G.: Extraction and clustering of motion trajectories in video. Proceedings, International Conference on Pattern Recognition **2** (2004) 521 – 524
57. Tipping, M.: The Relevance Vector Machine. Advances in Neural Information Processing Systems (1999) 652 – 658
58. Su, C., Zhuang, Y., Huang, L., Wu, F.: A two-step approach to multiple facial feature tracking: Temporal particle filter and spatial belief propagation. Proc. IEEE Intl Conf. on Automatic Face and Gesture Recognition (2004) 433 – 438
59. Pantic, M., Patras, I.: Dynamics of Facial Expressions-Recognition of Facial Actions and their Temporal Segments from Face Profile Image Sequences. IEEE Trans. Systems, Man and Cybernetics Part B **36** (2006) 433 – 449